

Visual-Relation Conscious Image Generation from Structured-Text

Duc Minh Vo[†]

vmduc@nii.ac.jp

Akihiro Sugimoto[‡]

sugimoto@nii.ac.jp

[†] SOKENDAI (The Graduate University for Advanced Studies), Japan

[‡] National Institute of Informatics, Japan

Abstract

Generating realistic images from text descriptions is a challenging problem and has many applications such as image editing or computer-aided design. In spite of recent progress on this text-to-image generation based on GANs, generating realistic images from complex descriptions with many entities in a general scene is not yet achieved in the literature. In the presence of multiple entities, the relationships between entities become important because they condition the location of each entity. We propose a GAN-based end-to-end network that learns the visual-relation layout between entities from given texts and conditions the layout in generating images. Our proposed network consists of the visual-relation layout module and the stacking-GANs. The visual-relation layout module predicts bounding-boxes for all the entities given in an input text so that each of them uniquely corresponds to each entity while keeping its involved relationships. The visual-relation layout is obtained by aggregating all the bounding-boxes, reflecting the scene structure given in text. The stacking-GANs is the stack of three GANs conditioned on the output of previous GAN and the visual-relation layout, consistently capturing the scene structure. Our network realistically renders entities' details in high resolution while keeping the scene structure. Experimental results on two public datasets show outperformances of our method against state-of-the-art methods.

1. Introduction

Generating photo-realistic images from text descriptions is one of important problems in computer vision. Besides having a wide range of applications such as intelligent image manipulation, it drives research progress in multimodal learning and inference across vision and language [1, 2, 3].

Recently proposed text-to-image generation methods [4, 5, 6, 7, 8] are based on conditional Generative Adversarial Networks (GANs) [9] and generate realistic images on limited domains such as descriptions of birds or flowers. Stack-

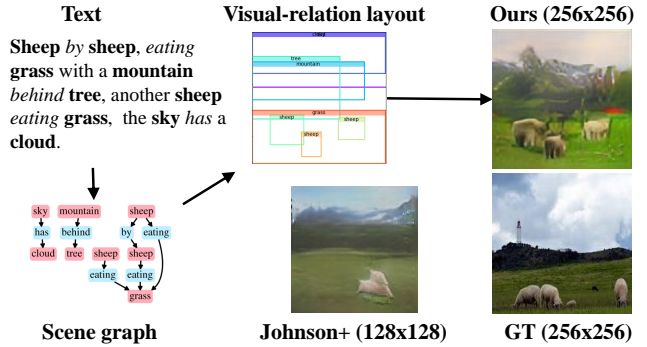


Figure 1: Example of generated images by our method. For comparison, we show the result by Johnson+[1] and the ground-truth. Scene graph and visual-relation layout are enlarged for best views.

ing such conditional GANs has shown even more ability of progressively rendering a more and more detailed entity in high-resolution [5, 8]. In general domains such as complex sentences with many entities and relationships, however, their performance becomes degraded. This is because they use only entity information in given text descriptions for realistically rendering a specific entity, leading to a poor layout of multiple entities in generated images.

In the presence of multiple entities, besides details of each entity, their layout in generated images becomes crucial for realistic image generation. Indeed, very recent work [1, 10] shows the effectiveness of inferring the scene layout from given text descriptions first. Johnson et al.[1] used scene graphs [2] to construct a scene layout by predicting bounding boxes and segmentation masks for all entities, which is then converted to an image. Hong et al.[10] constructs a semantic layout, a scene structure based on object instances, from input text descriptions and converts the layout into an image. However, their methods do not explicitly use relationship information between entities given in text description when inferring the layout, meaning the predicted bounding-boxes do not preserve the relation among

entities well. Localizing entities faithfully preserving their relationships given in text descriptions is desired.

We leverage advantages of stacking-GANs and inferring the scene layout, proposing a GAN-based end-to-end network for text-to-image generation where the network has two steps: (1) inferring from input text the *visual-relation layout*, i.e., the scene layout that preserves relationships between entities for entity localization, and (2) progressively generating coarse-to-fine images with stacking-GANs conditioned on the visual-relation layout. In the first step, our network predicts relation bounding-boxes for each entity in an input text depending on its involved relationship to other entities where we detect *subject-predicate-object* relationships between entities from an input text using its scene graph [2]. We then unify all the relation bounding-boxes into refined bounding-boxes so that each of them uniquely corresponds to one entity while keeping their relationships (in location and size) that are consistent with the text. Aggregating the refined bounding-boxes allows us to infer the visual-relation layout reflecting the scene structure given in the text. In the second step, on the other hand, three GANs progressively generate images in which entities are rendered in more and more details while keeping the scene structure. At each level, a GAN is conditioned on the visual-relation layout and the output of its previous GAN. Our network is learned in a fully end-to-end manner. Different from [1, 10], our proposed method explicitly employs *subject-predicate-object* relationships for predicting bounding-boxes so that they surely preserve the visual relation among entities.

The contribution of the proposed method is two-folds. (1) We propose the visual-relation layout in which entities are localized to preserve *subject-predicate-object* relationships between entities given in text descriptions. The visual-relation layout defines the scene structure for multiple entities that is consistent with text descriptions. (2) By conditioning stacking-GANs on the visual-relation layout, our method is able to progressively reproduce realistic detailed entities keeping their relationships from complex text descriptions. Experimental results on two public datasets (COCO-stuff [11] and Visual GENOME [12]) demonstrate outperformance of our method against state-of-the-arts (Fig. 1 shows an example).

2. Related work

Recent conditional GAN-based methods have shown promising results on text-to-image generation task [1, 4, 5, 7, 8, 10, 13]. Reed et al. [4] first proposed an end-to-end model that generates images using text embeddings extracted from the pre-trained text encoder [6]. Reed et al. [13] extended this work by proposing a GAN conditioned on both text and location information. Dong et al. [7] combined text and source image to compensate background information missing in text descriptions. Xu et al. [8] pro-

posed attentional GAN that fully uses global and local features in texts to generate detailed images. To render a more detailed entity, Zhang et al. [5] proposed to stack GANs conditioned on the result from a previous GAN and text, progressively generating high resolution images detailing an entity in text. Xu et al. [8] also used a stacking-GANs to generate images. They, however, struggle to faithfully reproduce complex sentences with many entities and relationships.

To overcome the limitation of GANs conditioned on text descriptions, a two-step approach was proposed where inference of the scene layout as an intermediate representation between text and image is followed by using the layout to generate images [1, 10]. Since the gap between the intermediate representation and image is smaller than that of text and image, this approach generates more realistic images. Chen et al. [14] proposed a method that generates high-resolution images using a semantic layout where the label of each entity is manually annotated to each pixel of the image to construct the layout. Hong et al. [10] proposed to infer a scene layout by feeding text descriptions into an LSTM. More precisely, they use an LSTM to predict bounding-boxes for all entities independently, and then employ a bi-directional convolutional LSTM to generate entity shapes from each predicted bounding-box without using any relationship information. The function of the bi-directional convolutional LSTM in their method is just the putting-together. Their method then combines the scene layout and text embeddings using the pre-trained text encoder [6], and uses a cascade refinement network (CRN) [14] for generating images. Johnson et al. [1], on the other hand, employed a scene graph [2] to predict a scene layout and then conditioned CRN [14] on the layout. The graph convolution network (GCN) used in this method aggregates relationship information of all the entities along the edges of the scene graph. At the end of GCN, however, the relationship information is lost because of the averaging operation on entity embeddings. Averaging entity embeddings means mixing different relationships in which a single entity is involved, resulting in failure of retaining each original relationship information. The layout constructed in these methods [1, 10] thus does not explicitly take into account relationships among entities for their localization, meaning the location of each entity may be independently predicted. As the result, their generated images may have poor scene structure as a whole even if each entity is realistically rendered. It is worth noting that neither [1] nor [10] is trained in the fully end-to-end manner. Indeed, [1] uses the ground-truth bounding-boxes to train the rendering part, and [10] trains their model step-by-step.

Different from above mentioned methods, our method constructs the visual-relation layout using *subject-predicate-object* relationships between entities extracted from an input text. Recursively conditioning stacking-

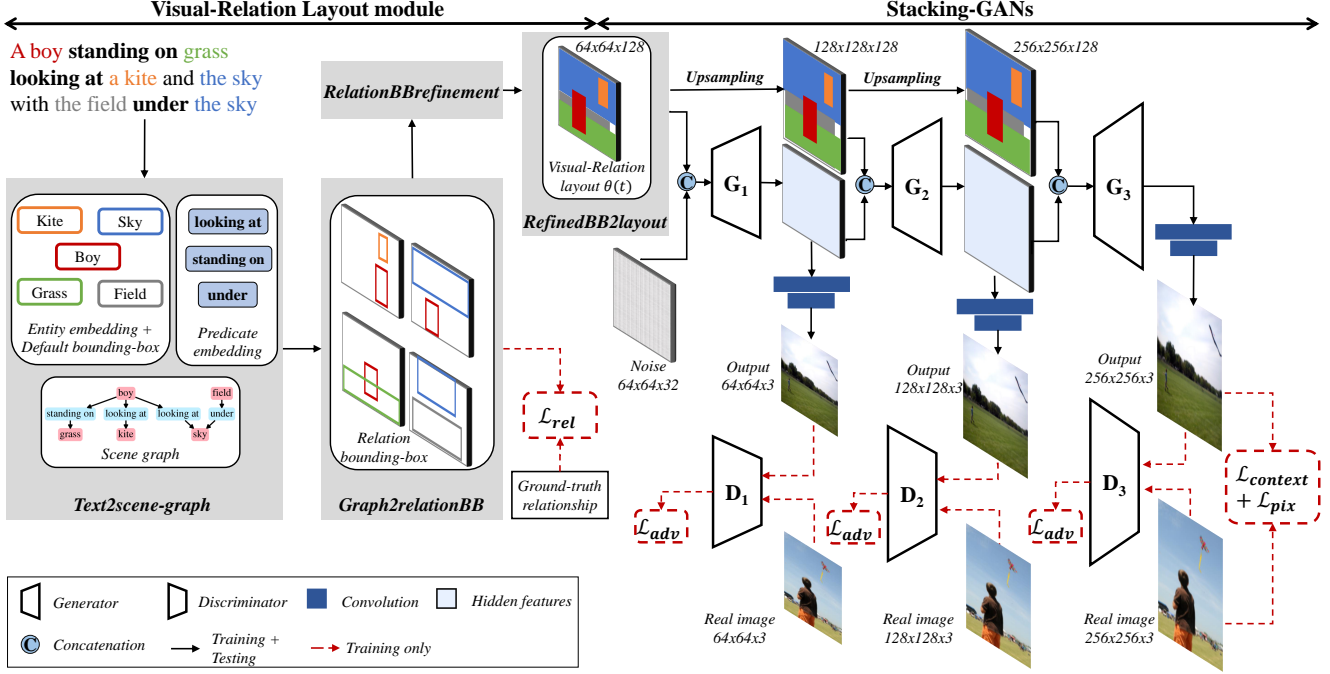


Figure 2: Framework of our proposed method.

GANs on our constructed visual-relation layout enables us to progressively generate coarse-to-fine images that consistently preserve the scene structure given in text.

3. Proposed method

Our method is decomposed into two steps: (1) inferring the visual-relation layout $\theta(t)$ from text description t , and (2) generating a realistic image from the visual-relation layout, namely $\hat{I} = G(\theta(t))$. To this end, we design an end-to-end network with two modules: the visual-relation layout module and the stacking-GANs.

Figure 2 illustrates our proposed network. It receives text description t as its input to progressively generate coarse-to-fine images \hat{I} 's with the size of $n \times n \times 3$ (n can be 64, 128, 256 depending on the GAN in the cascade; 3 are for RGB). The visual-relation layout module firstly converts t into its scene graph [2] and compute embeddings of all the entities and predicates appearing in the graph, using the *text2scene-graph subnet*. Note that any entity embedding is associated with a single default bounding-box. Next, the module predicts all relation bounding-boxes using the *graph2relationBB subnet*, and then unifies the relation bounding-boxes corresponding to the same entity to one refined bounding-box using the *relationBBrefinement subnet*. It finally aggregates refined bounding-boxes for $\theta(t)$ using the *refinedBB2layout subnet*. The stacking-GANs, on the other hand, consists of three GANs where each of them is conditioned on $\theta(t)$ and Gaussian noise (the first GAN) or

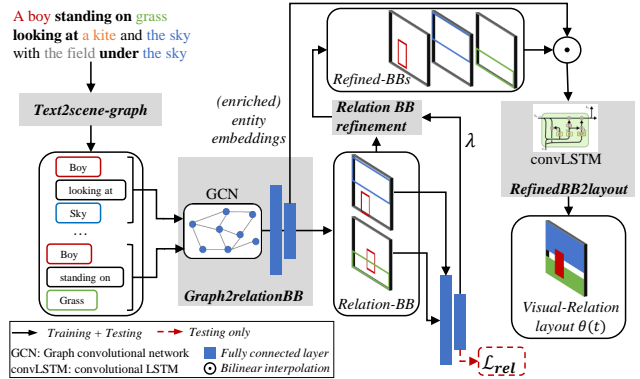


Figure 3: Details of visual-relation layout module (we omit the text2scene-graph subnet). This figure illustrates the prediction for two *subject-predicate-object* relationships.

hidden features of its previous GAN (the second and third GANs). We train the network in a fully end-to-end manner.

3.1. Visual-relation layout module

The goal of the visual-relation layout module is to construct the visual-relation layout $\theta(t)$ from a given text description t (Fig. 3). To this end, the visual-relation layout module should have ability of understanding entities and their relationships given in t . We convert t into its scene graph [2], i.e., the collection of *subject-predicate-object*'s. Each *subject-predicate-object* gives two kinds of

information: two entities and their relationship (in terms of predicate). The graph2relationBB subnet in this module predicts two relation bounding-boxes for each *subject–predicate–object*. Since each entity may participate in multiple relationships, we introduce the relationBBrefinement subnet to unify relation bounding-boxes so that each entity uniquely has a single refined bounding-box that is adjusted in location and size using all the relationships. The refinedBB2layout subnet then constructs the visual-relation layout by aggregating all the refined bounding-boxes together using convolutional LSTM.

Text2scene-graph subnet. This subnet receives a given text description t as its input and outputs embeddings of all the entities and predicates appearing in the text.

As the pre-processing, we borrow [1] to convert t to its scene graph (E, P) where $E \subseteq \mathcal{C}$ and $P \subseteq \mathcal{C} \times \mathcal{R} \times \mathcal{C}$. \mathcal{C} and \mathcal{R} are the set of categories and the set of relationships given in a dataset. An edge of (E, P) is associated with one *subject–predicate–object*. It is directed and represented by (e^s, p, e^o) with entities $e^s, e^o \in E$ and predicate $p \in \mathcal{R}$ (s and o indicate subject and object).

Following the learned embedding layer of the pre-trained word2vec model [15] (implemented in [16]), for a given scene graph (E, P) , we produce the entity embedding with the size of $1 \times |\mathcal{C}|$ and the predicate embedding with the size of $1 \times |\mathcal{R}|$ for any of all the entities and predicates appearing in (E, P) . Any entity embedding is associated with a single default bounding-box presented by $[x, y, w, h] \in [0, 1]^4$ where x is the *left coordinate*, y is the *top coordinate*, w is *width*, and h is *height*. We set $x = y = 0$ and $w = h = 1$ as the default. This process ensures that all the entities surely appear in the image. In the implementation, we concatenate the default bounding-box and its associated entity embedding to produce the vector with the size of $1 \times (|\mathcal{C}| + 4)$.

Graph2relationBB subnet. This subnet predicts all relation bounding-boxes for all the entities appearing in P with enriching the entity embeddings. We borrow GCN used in [1], which consists of five graph convolution layers where each of them is a stack of two fully-connected layers. Different from [1], each graph convolution layer in this subnet produces 512 and 388 outputs to process not only entity/predicate embeddings but also its corresponding bounding-boxes. On top of GCN, we add two more fully-connected layers producing 512 and 264 outputs to further aggregate the *subject–predicate–object* information and its corresponding bounding-boxes. Each fully-connected layer is followed by a ReLU layer [17].

For each edge k of scene graph (E, P) , the triplet of its embeddings (e_k^s, p_k, e_k^o) and default corresponding bounding-boxes with the size of $1 \times (|\mathcal{C}| + |\mathcal{R}| + |\mathcal{C}| + 8)$ are processed to give *enriched* subject $e_k'^s$, object $e_k'^o$ embeddings with the size of 1×128 each, separately, and their corresponding relation bounding-boxes b_k^s and b_k^o while keeping their relationship. Each relation bounding-box is

associated embedding $e_k'^s$ or $e_k'^o$ depending on “subject” or “object”. The number of relation bounding-boxes is $|\{b_k^s, b_k^o\}| = 2 \times |P|$ in total.

RelationBBrefinement subnet. Since one entity may participate in multiple relationships, we unify all the relation bounding-boxes corresponding to the same entity into one refined bounding-box. The relationBBrefinement subnet takes this role.

For entity $e_i (\in E)$, let $B_i = \{B_{i\nu}\}$ denote the set of its corresponding relation bounding-boxes and $\lambda_i = \{\lambda_{i\nu}\}$ be the set of their weights (we use B_i (capital letter) when specifying the bounding-box by entity).

We define the refined bounding-box \hat{B}_i of entity e_i by $\hat{B}_i = \sum_{\nu=1}^{|B_i|} (1 + \lambda_{i\nu}) \times B_{i\nu} / \sum_{\nu=1}^{|B_i|} (1 + \lambda_{i\nu})$. Each weight in λ_i is obtained from the outputs of the softmax function in the relationship auxiliary classifier using the relationship loss \mathcal{L}_{rel} (see Section 3.3 for details).

At the beginning of training, the relation bounding-boxes cannot exactly reproduce their involved relationships. Their weights thus tend to be close to *zero*, leading the bounding-boxes refinement operation almost similar to averaging. Although our refined bounding-boxes may be close to those of [1] at the beginning, ours still keep their relationships thanks to their weights.

As training proceeds, however, the weight of a relation bounding-box precisely retaining its relationships gradually increases, meaning that the contribution of the relation bounding-box to the refined bounding-box becomes larger and larger. As the result, the refined bounding-box is gradually adjusted in location and size, resulting in preserving relationships consistent with t .

For entity e_i , we also update its embedding by averaging the embeddings that are associated with $\{B_{i\nu}\}$ ’s over ν , so that \hat{B}_i is associated with the updated embedding.

In this way, we obtain the set of refined bounding-boxes $\{\hat{B}_i\}$ and their associated embeddings for all the entities in E . We remark that $|\{\hat{B}_i\}| = |E|$.

RefinedBB2layout subnet. In order to construct the visual-relation layout, we aggregate all the refined bounding-boxes and transfer them from the bounding-box domain to the image domain. This process should meet two requirements: (i) each entity should be localized and resized in the image to match its individual refined bounding-box, and (ii) the number of entities should be the same as that in the text description (in other words, it should be guaranteed that all the entities appear in the image even if some refined bounding-boxes overlap with each other). To this end, we design *refinedBB2layout* subnet as a learnable network rather than the putting-together operation as in [1]. We build this subnet using a convolutional LSTM [18] with the 5 hidden states outputting 128 channels each.

For refined bounding-box \hat{B}_i of entity e_i , we first convert it to the binary mask with the size of $64 \times 64 \times 128$ whose element is 1 iff it is contained in the (refined) bounding-box, 0

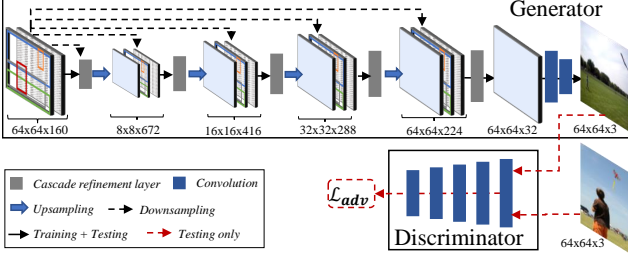


Figure 4: Details of one GAN in the stacking-GANs. Note that this figure illustrates the first GAN which receives the visual-relation layout ($64 \times 64 \times 128$) and Gaussian noise ($64 \times 64 \times 32$) as its input. The second (the third) GAN receives the upsampled visual-relation layout and the hidden features of previous GAN as its input.

otherwise. Then, we reshape its associated embedding from 1×128 to $1 \times 1 \times 128$. Finally, the reshaped embedding is wrapped to \hat{B}_i using the bilinear interpolation [19] for the layout of entity e_i whose size is $64 \times 64 \times 128$. To produce $\theta(t)$, we feed the sequence of entity layouts into the *refinedBB2layout* subnet. The size of $\theta(t)$ is $64 \times 64 \times 128$.

3.2. Stacking-GANs

We employ a stacking-GANs to progressively generate coarse-to-fine images. Our stacking-GANs consists of three GANs, each of which is conditioned on $\theta(t)$ (Fig. 4).

Each GAN consists of one generator to generate an image with the size of $n \times n \times 3$ ($n = 64, 128, 256$) and one discriminator to judge whether the generated image is real or fake. All the generators has the same architecture and all the discriminators has the same architecture, except for the image resolution. Parameters are not shared by any generators or discriminators.

Generator. Our generator consists of five refinement layers [14] producing 512, 256, 128, 64, 32 outputs and two convolution layers outputting 32 and 3 channels.

We concatenate $\theta(t)$ and Gaussian noise (for the first generator) or the hidden features (the output of the last refinement layer) of the previous generator (for the second and the third generators) to produce the input of $l \times l \times 160$ ($l = 64, 128, 256$). The size of $\theta(t)$ and the hidden features is upsampled using the bilinear interpolation [19] to be consistent with that of the generator input. At each level of refinement layers of each generator, the generator input is downsampled and concatenated with the output of the previous refinement layer (upsampled using the bilinear interpolation) to produce the input (except for the first refinement layer which receives the generator input only).

Discriminator. Following [9], we design our discriminator as the classification task rewarding high probability for real images and low one for generated images. Our discriminator consists of five convolution layers, outputting 64, 128,

256, 512, and 4 channels, respectively.

To prevent a discriminator from quickly converging, we add the noise instance [20] to the input image before feeding into the discriminator.

3.3. Loss function

We jointly train our network in an end-to-end manner with four losses: relationship loss, pixel loss, contextual loss, and adversarial loss.

Relationship loss \mathcal{L}_{rel} encourages relation bounding-boxes to keep their relationship. To compute \mathcal{L}_{rel} , we employ cross entropy between relation bounding-boxes and their ground-truth relationship that is obtained through the relationship auxiliary classifier.

We design our relationship auxiliary classifier is a stack of two fully-connected layers producing 512 and $|\mathcal{R}|$ outputs. The first fully-connected layer is followed by a ReLU layer while the second one ends with the *softmax* function.

For edge k of (E, P) , we concatenate e_k^{rs} , b_k^s , b_k^o , and e_k^{ro} in this order to have an input vector of 1×264 . We then feed this vector to the relationship auxiliary classifier, producing an output vector of $1 \times |\mathcal{R}|$. This output vector predicts the probability distribution w_k of relationships over \mathcal{R} . We first detect the predicate (i.e., relationship) p_k ($\in \mathcal{R}$) from k , and then identify the position of p_k in the allocation of w_k . Next, we set the output value at the position as the weight (used in the relationBBrefinement subnet) for b_k^s and b_k^o .

We use cross-entropy to compute the relationship loss: $\mathcal{L}_{rel} = -\sum_{k=1}^{|\mathcal{P}|} \sum_{\nu'=1}^{|\mathcal{R}|} p_k[\nu'] \log(w_k[\nu'])$.

Here we use embedding p_k for p_k because p_k faithfully retains relationship information given in text. Since the relationship reflects the relative distance among its associated relation bounding-boxes, minimizing the relationship loss encourages the relation bounding-boxes to adjust their locations and sizes to meet the “predicate” relationship.

Pixel loss: $\mathcal{L}_{pix} = ||I - \hat{I}||_2$, where I is the ground-truth image and \hat{I} is a generated image. The pixel loss is useful for keeping the quality of generated images.

Contextual loss [21] measures the similarity between images based on both context and semantics. Since refined bounding-boxes may lose the context of an image such as missing pixel information or the size of entity, we employ the contextual loss between I and \hat{I} to learn the context of an image.

Following [21], we define the contextual loss as: $\mathcal{L}_{context} = -\log(CX(\Phi^l(I), \Phi^l(\hat{I})))$,

where $\Phi^l(\cdot)$ denotes the feature map extracted from layer l of perceptual network Φ , and $CX(\cdot)$ is the function that computes the similarity between image features (see [21] for details).

Adversarial loss [9] is used to encourage the stacking-GANs to generate realistic images. In each GAN, training the generator and the discriminator is an adversarial learning process. We train the discriminator to re-

ward high scores for real images and low ones for generated images by maximizing the adversarial loss: $\mathcal{L}_{\text{adv}} = \mathbb{E}_{x \sim p_{\text{data}}}[\log D(x)] + \mathbb{E}_{x \sim p_{\text{gen}}}[(1 - \log D(x))]$,

where p_{data} and p_{gen} denote the training and the generated data, $D(\cdot)$ is the output of the discriminator, $\mathbb{E}_{(x) \sim p_{\text{data}}}$ and $\mathbb{E}_{x \sim p_{\text{gen}}}$ means the expectation over p_{data} and p_{gen} . The generator, on the other hand, is trained to minimize $\mathbb{E}_{x \sim p_{\text{gen}}}[(1 - \log D(x))]$ in \mathcal{L}_{adv} . In practice, however, to avoid vanishing gradients, the generator is trained to maximize $\mathbb{E}_{x \sim p_{\text{gen}}}[\log D(x)]$ [9].

In summary, our loss function is defined as

$$\mathcal{L} = \mathcal{L}_{\text{rel}} + \mathcal{L}_{\text{pix}} + \mathcal{L}_{\text{context}} + \sum_{i=1}^3 \mathcal{L}_{\text{adv}i}. \quad (1)$$

We remark that we compute \mathcal{L}_{adv} at each level in the stacking-GANs, while \mathcal{L}_{pix} and $\mathcal{L}_{\text{context}}$ are computed at the last level in the stacking-GANs.

4. Experiments

4.1. Dataset and compared methods

Dataset. We evaluated our method on the 2017 COCO-stuff dataset [11] and the Visual GENOME dataset [12]. Note that we followed [1] to pre-process all the datasets.

Compared methods. We employed Johnson+ [1] as the baseline. We also compared our method with Hong+ [10], Zhang+ [5], and Xu+ [8]. For Johnson+ [1], we used the pre-trained models [22] on both the datasets provided by the authors, and resized the generated images in order to produce high-resolution images. For Hong+ [10], we report the result in their paper because the implementation and pre-trained models are not publicly available. For Zhang+ [5] and Xu+ [8], we used the pre-trained models [23] and [24] on the COCO-stuff dataset while trained models from scratch on the GENOME dataset.

Evaluation metrics. We use the inception score (IS) [25] and Fréchet inception distance (FID) [26] to evaluate the overall quality of generated images. We also use four metrics to evaluate the visual-relation layout: the entity recall at IoU threshold ($R@ \tau$), the relationship IoU ($rIoU$), the relation score (RS), and the bounding-box coverage. To evaluate the relevance of generated image and input text description, we use the image caption task and report three standard language similarity metrics: *BLEU* [27], *METEOR* [28] and *CIDEr* [29].

To evaluate how much the predicted layout is consistent with the ground-truth, we measure the agreement in size and location between predicted (i.e., refined) and ground-truth bounding-boxes using the entity recall at IoU threshold: $R@ \tau = |\{i \mid IoU(\hat{B}_i, GT_i) \geq \tau\}|/N$, where \hat{B}_i and GT_i are predicted and ground-truth bounding-boxes for entity e_i , $N = \min(|\{\hat{B}_i\}|, |\{GT_i\}|)$ (we always observed $|\{\hat{B}_i\}| = |\{GT_i\}|$), τ is a IoU threshold, and $IoU(\cdot)$ denotes Intersection-over-Union metric. We remark that we

used only the bounding-boxes that exist in both $\{\hat{B}_i\}$ and $\{GT_i\}$ to compute $R@ \tau$.

We also evaluate the predicted layout using *subject-predicate-object* relationships. For each *subject-predicate-object* relationship, we computed the IoU of the predicted “subject” bounding-box and its corresponding ground-truth, and that for the “object”. We then multiplied the two IoUs to obtain the IoU for the relationship. $rIoU$ is the average over all the *subject-predicate-object* relationships.

We use the relation score (RS) [30] for COCO-stuff to evaluate the compliance of geometrical relation between predicted bounding-boxes. For each edge k of scene graph (E, P) , we define $score(\hat{B}_k^s, \hat{B}_k^o) = 1$ iff the relative location between \hat{B}_k^s and \hat{B}_k^o satisfies the relationship p_k , 0 otherwise. $RS = \sum_{k=1}^{|P|} score(\hat{B}_k^s, \hat{B}_k^o) / |P|$.

To evaluate how much bounding-boxes cover the area of the whole image, we compute the coverage of predicted bounding-boxes over the image area: $coverage = \bigcup_{i=1}^{|E|-1} \hat{B}_i / (\text{image area})$.

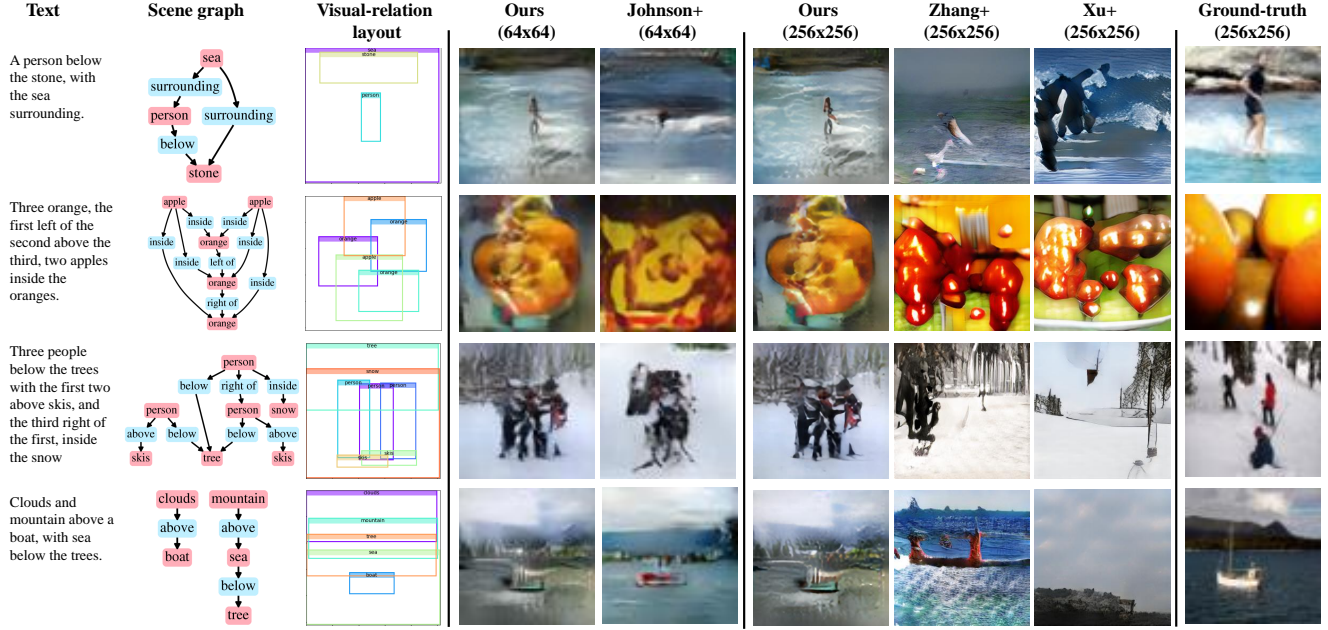
4.2. Implementation and training details

We implemented our model in PyTorch [16] and optimized on a PC with GTX1080Ti $\times 2$ using Adam optimizer with the recommended parameters [31] and batch size of 16 for 500 epochs. We used VGG-19 [32] pre-trained on ImageNet without any fine-tuning as Φ , and $l = conv4.2$ to compute $\mathcal{L}_{\text{context}}$.

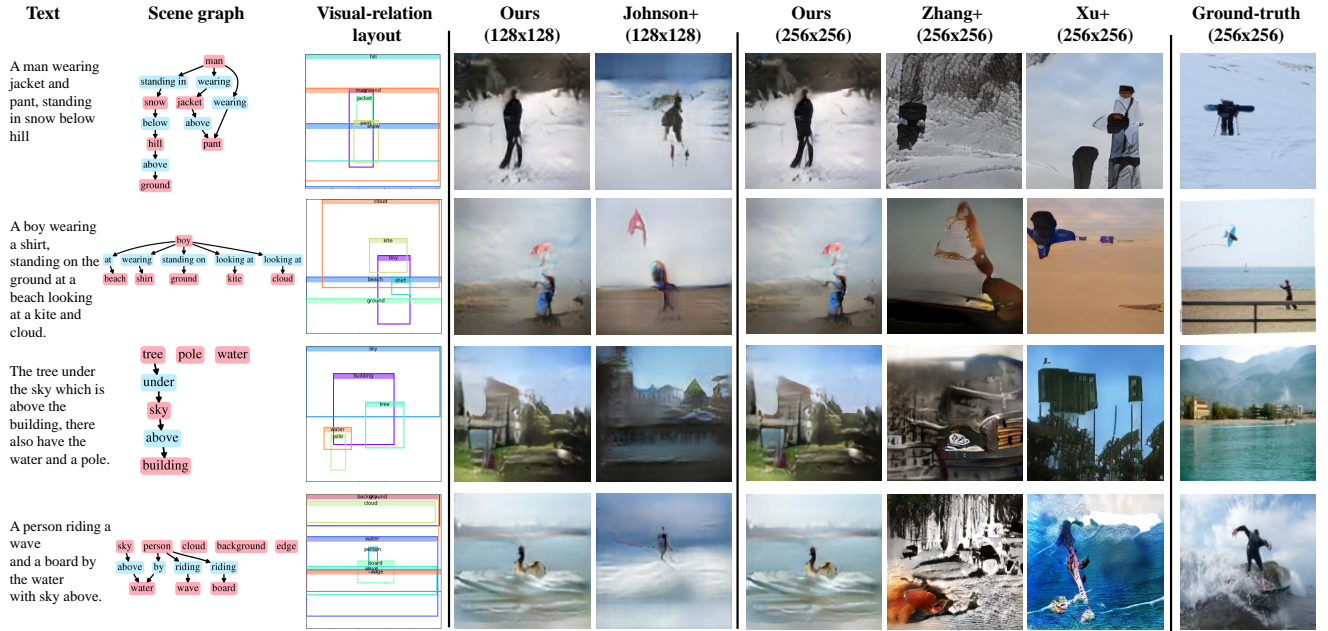
We trained all the subnets except for the *text2scene-graph* subnet, which is fixed, in the end-to-end manner where no hyperparameters are used for the weight control of loss terms and each individual subset does not need pre-training, meaning that our model does not use any ground-truth bounding-boxes to train the visual-relation layout. The visual-relation layout receives signals not only directly from the relationship loss but also from the other losses. In an early stage of the training, the rendering part cannot generate reasonable images because the quality of bounding-boxes is poor. This means the signals from losses are strong, leading to quick convergence of the layout generator. As the training proceeds, the layout generator properly works, and the rendering part gradually becomes better. The relationship loss, at that time, keeps the layout generator stable and more accurate.

4.3. Comparison with state-of-the-arts

Qualitative evaluation. Fig. 5 shows examples of the results obtained by our method and state-of-the-arts [1, 5, 8]. It shows that the generated images by our method successfully preserve the scene structure given in text descriptions. The results by our method also show the effectiveness of the stacking-GANs for high-resolution image generation because as the resolution becomes higher, more details of entities are reproduced.



(a) COCO-stuff dataset.



(b) GENOME dataset.

Figure 5: Visual comparison of our method against Johnson+ [1], Zhang+ [5] and Xu+ [8] on COCO-stuff [11], and GENOME [12]. In the first block, from left to right, a text description, its scene graph, and our visual-relation layout. The last block shows the ground-truth image in the datasets. Scene graphs and Visual-relation layouts are enlarged for best views. (Quality of generated images in different resolution can be clearly observed by enlarging the PDF.)

On COCO-stuff (Fig. 5a), we see that although some details in our results are not clear, the scene structure of our results are highly consistent with that of the ground-truths. For examples, in the first and third rows, the locations of entity “person” predicted by our method are the same with

those in the ground-truth images. We see that the results by Johnson+[1] have reasonable layouts, however, the visual impression of their results is not good. The results by Zhang+[5] and Xu+[8], on the other hand, are clear in details (entities) but they lose the scene structure (some enti-

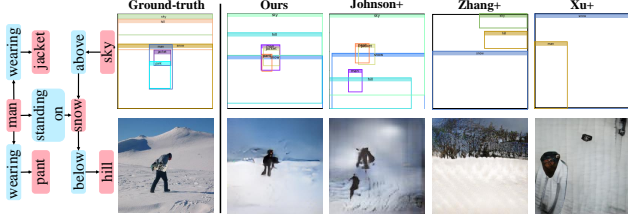


Figure 6: Example of predicted layouts with generated images by our method, Johnson+ [1], Zhang+ [23], and Xu+ [8] on GENOME [12]. The first block shows scene graph and ground-truth. In the second block, from above to below, layout and generated image by each method. (Enlarged for best view).

ties disappear).

On GENOME (Fig. 5b), we see similar observation. Our results are better in entity detail and scene structure than the others. In particular, for complex sentences (first and second rows), our results faithfully preserve the scene structure given in text thanks to our visual-relation layout.

Fig. 6 shows an example of predicted layouts by all methods. Our method predicts more precise layout than the others. Although the layout by Johnson+ [1] seems reasonable to some extent, some entities lose their relation (manwearingjacket, snowbelowhill, etc.). The layouts by Zhang+ [23] and Xu+ [8] do not reflect the scene structure.

Quantitative evaluation. To quantitatively evaluate the overall quality of results, we computed IS and FID of generated images using the implementation in [33, 34].

Table 1 shows that our method outperforms Johnson+ [1] in IS on both COCO-stuff and GENOME. We also see that along with the stacking-GANs, our method achieves better scores. Our method does not outperform Hong+ [10], Zhang+ [5], and Xu+ [8] in IS . This can be explained as follows. Hong+[10] focuses on detailing entities by generating a fine shape for each entity and then putting all the shapes together before feeding into the rendering part. Zhang+[5] and Xu+[8] focus on generating images in good human perception based on entity information. As the result, the entities in the generated images are more detailed than those in our results in the sense of human perception. Their results, however, have poor layouts as seen later in Table 2. Rendering entities in more details by our method is left for future work.

Table 1 also shows that our method achieves second to the best on COCO-stuff and the best on GENOME in FID , meaning that the distribution of our generated images is closer to that of real data when compared with the others.

We classify all the methods whose models are publicly available into two: (A) ours and Johnson+ [1] (which are conditioned on the layout), and (B) Zhang+ [5] and Xu+ [8] (which are conditioned on texts). Tables 1 shows (A) has

worse IS scores than (B); (A), however, can generate images whose distribution is closer to the real data (better FID on the GENOME dataset) thanks to the faithful scene structure (as seen later in Table 2). We may thus conclude that inferring the scene layout before generating images is more effective and promising in dealing with even complex descriptions.

Next, we evaluated how the scene structure given in input text is preserved in generated images. For this evaluation, we computed $R@τ$ (we changed $τ$ from 0.3 to 0.9 by 0.2), $rIoU$, RS , and $coverage$, see Table 2. We remark that we computed RS only for COCO-stuff because COCO-stuff has geometrical relationships only. Since Zhang+[5] and Xu+[8] do not predict any bounding-boxes in their methods, we employed Faster-RCNN [35] to estimate their predicted bounding-boxes of entities where we set the number of generated bounding-boxes to be the number of entities in an image. We note that the number of predicted bounding-boxes by ours or Johnson+[1] was always the same with the number of entities in an image.

Table 2 shows that our method performs best, meaning that our predicted bounding-boxes more precisely agree with those in relationship (location and size) of entities given in text. We can thus conclude that the scene structure in our results is more precise than that in the other methods. This promises the improvement in quality of our generated images because with more precise bounding-boxes, more realistic images can be generated [14].

From $rIoU$'s in Table 2, we see that our predicted bounding-boxes more successfully retain the relationships of entities than the other methods. This observation is also supported by RS on COCO-stuff. Moreover, our method outperforms the others in $coverage$ and achieves comparable levels with the ground-truth bounding-boxes. These indicate our visual-relation layout is well-structured. Our method thus has ability of rendering more realistic images than the other methods since the faithful scene structure and more bounding-box coverage (i.e., entity information) are important in the presence of multiple entities. We also see that the $coverage$'s on COCO-stuff are better than those on GENOME, which explains the reason why generated images on COCO-stuff are better in IS and FID .

Finally, we use the image caption task to evaluate how the generated image is relevant to its input text. To this end, we first employ a pre-trained image caption generator [36] on COCO-stuff [11] to generate one caption per generated image. We then measure the similarity between the input text description and the predicted sentence using $BLEU$ [27], $METEOR$ [28] and $CIDEr$ [36] (Table 3). We remark that we only evaluated on COCO-stuff since the pre-trained image caption generator on GENOME is not available.

Table 3 our method outperforms the others [1, 10] on $BLEU$ and comparable to [10] on $METEOR$ and

Table 1: Comparison of the overall quality using *IS*. (larger is better) and *FID* (smaller is better). Scores inside the parentheses indicate those reported in the original papers.

Dataset	IS						FID					
	COCO-stuff [11]			GENOME [12]			COCO-stuff [11]			GENOME [12]		
Image size	64 × 64	128 × 128	256 × 256	64 × 64	128 × 128	256 × 256	64 × 64	128 × 128	256 × 256	64 × 64	128 × 128	256 × 256
Ours w/o relationBBrefinement	6.63±0.17	6.71±0.20	6.88±0.19	4.89±0.11	4.97±0.14	5.04±0.09	66.14	60.17	52.35	81.02	78.58	72.15
Ours w/o refinedBB2layout	6.22±0.27	6.47±0.31	6.51±0.24	4.63±0.17	4.81±0.14	4.89±0.19	89.05	84.66	80.31	82.57	80.91	79.02
Ours with GT layout	7.72±0.28	8.36±0.22	9.10±0.30	6.21±0.09	6.93±0.15	7.51±0.19	47.50	38.71	33.29	60.53	52.12	47.63
Ours w/o \mathcal{L}_{pix}	5.77±0.19	5.93±0.13	6.19±0.16	3.75±0.13	3.90±0.17	4.28±0.21	87.16	85.01	80.18	85.19	83.77	80.01
Ours w/o $\mathcal{L}_{context}$	5.89±0.17	5.99±0.27	6.22±0.24	3.81±0.15	4.02±0.20	4.33±0.19	85.18	81.63	80.37	83.74	79.24	77.45
Ours w/o \mathcal{L}_{adv}	5.61±0.30	5.79±0.22	6.01±0.25	3.77±0.17	3.99±0.11	4.29±0.10	105.16	95.11	91.22	97.62	87.36	81.96
Ours (completed model)	7.23±0.21	7.86±0.18	8.03±0.26	5.24±0.15	5.89±0.17	6.31±0.11	53.97	44.66	41.02	70.47	66.13	63.89
Johnson+ [1]	6.51±0.41 (6.70±0.10)	5.99±0.27	5.89±0.34	5.08±0.15 (5.5±0.10)	4.78±0.15	3.70±0.12	67.99	95.18	102.41	73.39	70.40	93.39
Hong+ [10]	(11.46±0.09)	—	—	—	—	—	—	—	—	—	—	—
Zhang+ [5]	7.79±0.32	8.49±0.52	9.81±0.41	6.35±0.16	6.44±0.25	7.39±0.38	87.21	85.37	78.19	108.68	86.17	77.95
Xu+ [8]	11.78±0.14	19.11±0.28	23.59±0.23	6.38±0.22	6.88±0.32	8.20±0.35	50.06	43.98	34.48	96.40	83.39	72.11
			(25.89±0.47)									
Ground-truth	16.25±0.38	25.89±0.47	32.61±0.69	13.92±0.42	21.43±1.03	31.22±0.65	—	—	—	—	—	—

Table 2: Comparison of the scene structure using $R@r$, $rIoU$, RS , and $coverage$. Scores are the averages over the test images (larger is better).

Dataset	COCO-stuff [11]					GENOME [2]							
Metric	$R@r$		$rIoU$	RS	coverage	$R@r$		$rIoU$	RS	coverage			
	0.3	0.5	0.7	0.9	(GT=98.24)	0.3	0.5	0.7	0.9	(GT=77.10)			
Ours w/o relationBBrefinement	60.18	43.27	29.76	20.33	0.2627	58.62	94.11	28.46	18.02	13.25	10.68	0.1473	54.09
Ours (completed model)	63.85	46.28	32.71	22.57	0.2911	70.01	96.88	31.07	20.71	14.87	12.02	0.1758	69.24
Johnson+ [1] (64 × 64)	59.75	42.53	29.23	19.89	0.2532	56.38	94.82	28.13	17.17	12.30	10.47	0.1485	52.28
Johnson+ [1] (128 × 128)								28.39	17.27	12.33	10.41	0.1378	52.45
Zhang+ [5]	37.81	20.50	10.64	7.76	0.0824	37.14	60.15	18.38	10.84	8.11	5.82	0.0643	40.07
Xu+ [8]	21.39	10.71	8.15	5.83	0.0671	39.25	52.76	16.02	9.33	7.66	5.15	0.0579	36.82

Table 3: Comparison using caption generation metrics on COCO-stuff (higher is better). Scores inside the parentheses indicate those reported in [10].

Method	$BLEU-1$	$BLEU-2$	$BLEU-3$	$BLEU-4$	$METEOR$	$CIDEr$
Hong+ [10]	(0.541)	(0.332)	(0.199)	(0.122)	(0.154)	(0.367)
Johnson+ [1]	0.531	0.321	0.183	0.107	0.141	0.238
Ours	0.553	0.346	0.209	0.131	0.153	0.317
Ground-truth	0.627	0.434	0.287	0.191	0.191	0.367
	(0.678)	(0.496)	(0.349)	(0.243)	(0.228)	(0.802)

CIDEr. Note that all the scores on ground-truth dataset in [10] are higher than our re-computation. We thus conclude our method performs best in consistency.

4.4. Ablation study

We evaluated the plausibility of employing the visual-relation layout module, see the first block of Tables 1, and 2. Here we used the ground-truth bounding-box layout, or replaced each subnet in the visual-relation layout module by a standard operation: model w/o relationBBrefinement denotes the replacement by just averaging all relation bounding-boxes; model w/o refinedBB2layout denotes the replacement by just putting all entity layouts together in constructing the visual-relation layout.

We see that each subnet in the visual-relation layout module contributes to the improvement of quality of generated images. In particular, the fourth row of Table 2 in-

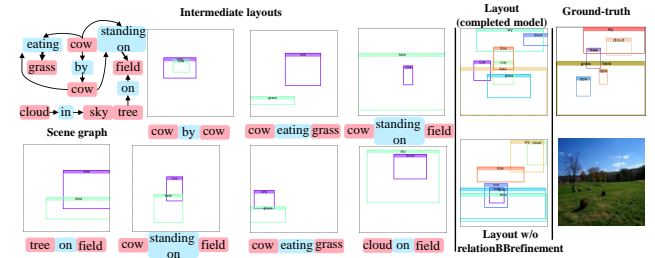


Figure 7: Example of relation BBs in graph2relationBB and layouts by w/ and w/o relationBBrefinement on GENOME. In the first block, scene graph and GT. In the second block, intermediate layouts obtained by graph2relationBB subnet and their *subject-predicate-object*. In the last block, the final layouts obtained by our completed model (above) and model w/o relationBBrefinement (below).



Figure 8: Example of generated images by our completed model and model w/o refinedBB2layout.

icates importance of the adjustment of relation bounding-boxes using weights coming from the relationship loss. This observation supports the necessity of the relationship loss. Fig. 7 shows the visual-relation layouts obtained by w/ and w/o relationBBrefinement. The layout by w/ relationBBrefinement reflects better relation among entities than w/o relationBBrefinement (some entities in w/o relationBBrefinement overlap). After graph2relationBB subnet, bounding-boxes can be diverse in size and location (the 2nd block in Fig. 7). We thus need relationBBrefinement for train-

able unification of the bounding-boxes. As illustrated in Fig. 8, model w/o refinedBB2layout does not work well when many entities are located close to each other in the descriptions and overlapping of their predicted bounding-boxes arises (we can see such overlapping in the visual-relation layout). We also see that employing ground-truth bounding-boxes boosts performance in both *IS* and *FID*, meaning that predicting accurate bounding-boxes is important.

We evaluated the necessity of each term of the loss function through comparing our completed model with models dropping one term each: model w/o \mathcal{L}_{pix} , model w/o $\mathcal{L}_{\text{context}}$, and model w/o \mathcal{L}_{adv} (we dropped each term in the loss function (1) except for stacking-GANs). From the second block of Table 1, we see that the absence of any term degrades the quality of generated images. This indicates that all the terms in the loss function indeed contribute to performance.

Finally, we discuss the impact of visual-relation layout and contextual loss on *IS* and *FID*. First, the contextual loss gives the feedback to visual-relation layout module, leading to a better layout (bounding-box in size and position). A better layout enables our render ([14]) to generate a better image in quality. Our method infers best layouts (Table 2). The rendering part also receives the feedback from the contextual loss to improve quality of generated images. These two factors together bring gain on *IS* and *FID*, leading better *IS* and *FID* scores than Johnson+ [1]. Since the visual-relation layout module receives the feedback from the contextual loss, dropping the contextual loss degrades the quality of inferred layouts as well. As a result, *IS* and *FID* scores become far worse than just dropping it.

5. Conclusion

We proposed a GAN-based end-to-end network for text-to-image generation where relationships between entities are used to infer a visual-relation layout and the stacking-GANs conditioned on the visual-relation layout generates high-resolution realistic images. Our visual-relation layout preserves the scene structure more precisely than the layout by state-of-the-arts. Experimental results on two public datasets demonstrate the effectiveness of our method.

References

- [1] J. Johnson, A. Gupta, and L. Fei-Fei, “Image generation from scene graphs,” in *CVPR*, 2018. 1, 2, 4, 6, 7, 8, 9, 10
- [2] J. Johnson, R. Krishna, M. Stark, J. Li, M. Bernstein, and L. Fei-Fei, “Image retrieval using scene graphs,” in *CVPR*, 2015. 1, 2, 3, 9
- [3] Y. Li, W. Ouyang, B. Zhou, K. Wang, and X. Wang, “Scene graph generation from objects, phrases and region captions,” in *ICCV*, 2017. 1
- [4] S. Reed, Z. Akata, X. Yan, L. Logeswaran, B. Schiele, and H. Lee, “Generative adversarial text-to-image synthesis,” in *ICML*, 2016. 1, 2
- [5] H. Zhang, T. Xu, H. Li, S. Zhang, X. Wang, X. Huang, and D. Metaxas, “Stackgan: Text to photo-realistic image synthesis with stacked generative adversarial networks,” in *ICCV*, 2017. 1, 2, 6, 7, 8, 9
- [6] S. Reed, Z. Akata, H. Lee, and B. Schiele, “Learning deep representations of fine-grained visual descriptions,” in *CVPR*, 2016. 1, 2
- [7] H. Dong, S. Yu, C. Wu, and Y. Guo, “Semantic image synthesis via adversarial learning,” in *ICCV*, 2017. 1, 2
- [8] T. Xu, P. Zhang, Q. Huang, H. Zhang, Z. Gan, X. Huang, and X. He, “AttnGAN: Fine-grained text to image generation with attentional generative adversarial networks,” in *CVPR*, 2018. 1, 2, 6, 7, 8, 9
- [9] I. Goodfellow, J. Pouget-Abadie, M. Mirza, B. Xu, D. Warde-Farley, S. Ozair, A. Courville, and Y. Bengio, “Generative adversarial nets,” in *NIPS*, 2014. 1, 5, 6
- [10] S. Hong, D. Yang, J. Choi, and H. Lee, “Inferring semantic layout for hierarchical text-to-image synthesis,” in *CVPR*, 2018. 1, 2, 6, 8, 9
- [11] H. Caesar, J. Uijlings, and V. Ferrari, “Coco-stuff: Thing and stuff classes in context,” in *CVPR*, 2018. 2, 6, 7, 8, 9
- [12] R. Krishna, Y. Zhu, O. Groth, J. Johnson, K. Hata, J. Kravitz, S. Chen, Y. Kalantidis, L.-J. Li, D. A. Shamma, M. Bernstein, and L. Fei-Fei, “Visual genome: Connecting language and vision using crowdsourced dense image annotations,” in *IJCV*, 2017. 2, 6, 7, 8, 9
- [13] S. Reed, Z. Akata, S. Mohan, S. Tenka, B. Schiele, and H. Lee, “Learning what and where to draw,” in *NIPS*, 2016. 2
- [14] Q. Chen and V. Koltun, “Photographic image synthesis with cascaded refinement networks,” in *ICCV*, 2017. 2, 5, 8, 10
- [15] T. Mikolov, I. Sutskever, K. Chen, G. Corrado, and J. Dean, “Distributed representations of words and phrases and their compositionality,” in *NIPS*, 2013. 4
- [16] <https://pytorch.org/>. 4, 6

- [17] V. Nair and G. E. Hinton, "Rectified linear units improve restricted boltzmann machines," in *ICML*, 2010. 4
- [18] X. Shi, Z. Chen, H. Wang, D.-Y. Yeung, W. kin Wong, and W. chun Woo, "Convolutional lstm network: A machine learning approach for precipitation nowcasting," in *NIPS*, 2015. 4
- [19] M. Jaderberg, K. Simonyan, A. Zisserman, and k. kavukcuoglu, "Spatial transformer networks," in *NIPS*, 2015. 5
- [20] C. K. Sønderby, J. Caballero, L. Theis, W. Shi, and F. Huszár, "Amortised MAP inference for image super-resolution," in *ICLR*, 2017. 5
- [21] R. Mechrez, I. Talmi, and L. Zelnik-Manor, "The contextual loss for image transformation with non-aligned data," in *ECCV*, 2018. 5
- [22] <https://github.com/google/sg2im>. 6
- [23] <https://github.com/hanzhanggit/StackGAN-Pytorch>. 6, 8
- [24] <https://github.com/taoxugit/AttnGAN>. 6
- [25] T. Salimans, I. Goodfellow, W. Zaremba, V. Cheung, A. Radford, X. Chen, and X. Chen, "Improved techniques for training gans," in *NIPS*, 2016. 6
- [26] M. Heusel, H. Ramsauer, T. Unterthiner, B. Nessler, and S. Hochreiter, "Gans trained by a two time-scale update rule converge to a local nash equilibrium," in *NIPS*, 2017. 6
- [27] K. Papineni, S. Roukos, T. Ward, and W.-J. Zhu, "Bleu: A method for automatic evaluation of machine translation," in *ACL*, 2002. 6, 8
- [28] A. Lavie and A. Agarwal, "Meteor: An automatic metric for mt evaluation with improved correlation with human judgments," in *ACL*, 2005. 6, 8
- [29] R. Vedantam, C. L. Zitnick, and D. Parikh, "Cider: Consensus-based image description evaluation." in *CVPR*, 2015. 6
- [30] S. Tripathi, A. Bhiwandiwalla, A. Bastidas, and H. Tang, "Using scene graph context to improve image generation," 2019. 6
- [31] D. P. Kingma and M. Welling, "Auto-encoding variational bayes," in *ICLR*, 2014. 6
- [32] K. Simonyan and A. Zisserman, "Very deep convolutional networks for large-scale image recognition," in *ICLR*, 2015. 6
- [33] https://github.com/openai/improved-gan/tree/master/inception_score. 8
- [34] <https://github.com/bioinf-jku/TTUR>. 8
- [35] S. Ren, K. He, R. Girshick, and J. Sun, "Faster R-CNN: Towards real-time object detection with region proposal networks," in *NIPS*, 2015. 8
- [36] C. Wang, C. Xu, C. Wang, and D. Tao, "Perceptual adversarial networks for image-to-image transformation," *IEEE Transactions on Image Processing*, 2018. 8